Journal of Materials Science: Materials in Electronics (2018) 29:12639–12651
https://doi.org/10.1007/s10854-018-9381-9

Very high thermal stability with excellent dielectric, and non-ohmics properties of Mg-doped $CaCu_3Ti_{4.2}O_{12}$ ceramics

Ekaphan Swatsitang[1,2] · Krissana Prompa[1] · Thanin Putjuso[3]

Received: 16 April 2018 / Accepted: 26 May 2018 / Published online: 29 May 2018

Abstract
In this work, the nominal $CaCu_{3-x}Mg_xTi_{4.2}O_{12}$ (0.00, 0.05 and 0.10) ceramics were prepared by sintering pellets of their precursor powders obtained by a polymer pyrolysis solution method at 1100 °C for different sintering time of 8 and 12 h. Very low loss tangent (tanδ) < 0.009–0.014 and giant dielectric constant (ε') ~ 1.1×10^4–1.8×10^4 with excellent temperature coefficient ($\Delta\varepsilon'$) less than ± 15% in a temperature range of − 60 to 210 °C were achieved. These excellent performances suggested a potent application of the ceramics for high temperature X8R and X9R capacitors. It was found that tanδ values decreased with increasing Mg^{2+} dopants due to the increase of grain boundary resistance (R_{gb}) caused by the very high density of grain, resulting from the substitution of small ionic radius Mg^{2+} dopants in the structure. In addition, $CaCu_{3-x}Mg_xTi_{4.2}O_{12}$ ceramics displayed non-linear characteristics with the significant enhancements of a non-linear coefficient (α) and a breakdown field (E_b) due to Mg^{2+}doping. The high values of ε' (14012), α (13.64) and E_b (5977.02 V/cm) with very low tanδ value (0.009) were obtained in a $CaCu_{2.90}Mg_{0.10}Ti_{4.2}O_{12}$ ceramic sintered at 1100 °C for 8 h.

1 Introduction

Presently, investigation for high performance capacitors with efficient operation in a wider temperature range, especially in a high temperature region, has been extensively attempted due to the increasing demand of the materials in automobile, aerospace and military mobile communications industries and etc. [1]. In addition to high dielectric constant (ε') and low loss tangent (tanδ) values, one important factor to be considered for good capacitor is the temperature stability of $\varepsilon'\left(\Delta\varepsilon' = 100\times(\varepsilon'_T - \varepsilon'_{30^\circ C})/\varepsilon'_{30^\circ C}\right)$ that must be less than ± 15% in a given temperature range, which is practically dissimilar for different types of capacitor. For instance, X9R, X8R and X7R capacitors are allowed to operate in a temperature range of − 55 to 200 °C, − 55 to 150 °C and − 55 to 125 °C, respectively. From literatures, a number of articles concerning the temperature stability study of capacitors have been mostly reported for X8R [2–5] and X7R [6] capacitors, but rarely for X9R capacitor [1, 7, 8]. Recently, in order to achieve the excellent $\Delta\varepsilon'$ that satisfies the categories for X9R capacitor, attempt have been proposed on various investigations by shifting the Curie temperature (T_c) in $BaTiO_3$-based materials and other ferroelectric materials of perovskite type [7–11], as for examples. However, some of these compounds are complex with Pb as a constituent that can be easily decomposed at a high sintering temperature during the preparation process and cause seriously environmental problems due to the toxicity of Pb.

Over the past decade, perovskite $CaCu_3Ti_4O_{12}$ (CCTO) [12–17] compounds with giant dielectric constant and other novel giant dielectric materials [18–20] have been comprehensively studied, focusing on high performance capacitor as well. In general, CCTO [21] exhibits an ultra-high dielectric permittivity (ε') without any detectable phase transition over a wide temperature range. In principle, the dielectric properties of CCTO strongly depend on the electrical heterogeneity of grains, consisting of *n*-type semiconducting grains and insulating grain boundaries (GBs) [15, 17, 22, 23] i.e. the grain and grain boundary resistances are crucial

✉ Thanin Putjuso
thanin.put@rmutr.ac.th

[1] Integrated Nanotechnology Research Center (INRC) and Department of Physics, Faculty of Science, Khon Kaen University, Khon Kaen 40002, Thailand

[2] Nanotec-KKU Center of Excellence on Advanced Nanomaterials for Energy Production and Storage, Khon Kaen University, Khon Kaen 40002, Thailand

[3] School of General Science, Faculty of Liberal Arts, Rajamangala University of Technology Rattanakosin, Wang Klai Kangwon Campus, Hua Hin, Prachuap Khiri Khan 77110, Thailand

factors that affect the dielectric properties. Recently, many researchers reported that several CCTO-based compounds had demonstrated themselves to accomplish a category for the EIA code X7R capacitor [24, 25]. Moreover, several groups had successfully prepared materials, which could be applied for X8R capacitor by co-doping CCTO [5, 26] and doping $Ca_2Cu_3Ti_4O_{12}$ (CCTO/$CaTiO_3$) [4] with some metals. To our knowledge CCTO-based ceramics with satisfactional properties for X9R capacitor have not been reported.

Differently, many groups have focused their work on the study of $CaCu_3Ti_4O_{12}/TiO_2$ ceramics with excess molar concentration of Ti. For instance, Lin et al. [27] reported the successful preparation of TiO_2-rich CCTO ($CaCu_3Ti_{4+x}O_{12}$; x = 0.00, 0.5, 1.00 and 1.5) ceramics through a solid state reaction process. In this report, it was found that TiO_2 secondary phase trended to increase with increasing Ti content, whereas ε' and tanδ values decreased to ~4233 and ~0.03, respectively. Furthermore, nonlinear characteristics could be improved. In the work of Ouyang et al. [28], it was reported that TiO_2 phase could modify the microstructural and electrical properties of CCTO ceramics prepared by a sol–gel process. At room temperature (RT) and 0.1 kHz, they found that these ceramic samples exhibited ε' value of $\sim 5.5 \times 10^4$ with tanδ value of ~0.2. Other than this, Hao et al. [29] had successfully prepared CCTO/$x$$TiO_2$ (x = 0.0, 0.5, 1.0 and 2.0) ceramics by a sol–gel process. They found that tanδ value at low frequency decreased with increasing Ti content, resulting from the presence of TiO_2 secondary phase. Moreover, ε' and tanδ values were relatively proportional to the amount of TiO_2. Although various CCTO/TiO_2-based ceramics have been widely studied, it was hard to fulfill all of the requirements for high dielectric performance, especially for the excellent value of $\Delta\varepsilon'$ in a properly given temperature range. However, it is evident that over all dielectric properties and $\Delta\varepsilon'$ of CCTO-based ceramics can be significantly improved by Mg^{2+} doping [30, 31] and co-doping with others metal [5, 26, 32]. For instance, very high performance dielectric properties with appropriate $\Delta\varepsilon'$ for X8R capacitor could be achieved by substitution of Mg^{2+} ions on the Cu^{2+} sites in the crystal structure of $Ca_2Cu_2Ti_4O_{12}$ ceramics [4]. According to these reports, it is interesting to put forward effort on the study of Mg^{2+}-doped $CaCu_2Ti_4O_{12}/TiO_2$ ceramics with the presumption that overall dielectric properties and temperature stability of the dielectric constant can be improved and benefit for the X9R capacitor. Therefore, it is the aim of this work to provide a different approach for the improvement of the overall dielectric properties with excellent $\Delta\varepsilon'$ of CCTO-based ceramics by substitution of Mg^{2+} ions into a binary compound system of $CaCu_{3-x}Mg_xTi_4O_{12}/TiO_2$ ceramics. In order to accomplish this, a well-established polymer pyrolysis solution method (PP method) has been employed for the preparation of high performance CCTO-based ceramics [33, 34]. In this work, $CaCu_{3-x}Mg_xTi_{4.2}O_{12}$ (x = 0.00, 0.05 and 0.10) precursor powders were prepared by a PP method. Effect of Mg^{2+} doping on the dielectric and non-ohmics properties, including the $\Delta\varepsilon'$ were examined and discussed based on the promotion of oxygen vacancy at GB. Surprisingly, very low loss tangent (tanδ < 0.009–0.014) and high dielectric constant ($\varepsilon' \sim 1.1 \times 10^4$–$1.8 \times 10^4$, at 1 kHz and RT) with excellent temperature stability less than ± 15% of $\Delta\varepsilon'$ over a more wider temperature range of − 60 to 210 °C were achieved. In addition, the highest value of α ~ 13.75 and E_b ~ 5977.0 V/cm were obtained. In order to clarify the effect of Mg^{2+} ions on the dielectric and non-ohmics properties of prepared ceramic samples, impedance measurements were performed.

2 Experimental details

$CaCu_{3-x}Mg_xTi_{4.2}O_{12}$ (x = 0.00, 0.05 and 0.10) precursor powders were prepared by a PP method. $Cu(NO_3)_2{\cdot}3H_2O$ (99.5% Carlo Erba), $Ca(NO_3)_2{\cdot}4H_2O$ (99.99% Kanto), $TiC_{16}H_{28}O_6$ (75 wt% in isopropanol), $Mg(NO_3)_2{\cdot}6H_2O$ (99.9% Kanto), $(NH_4)_2S_2O_4$ (99.95% Carlo Erba) and acrylic acid were used as starting materials. The complete details for the preparation of these powders were given elsewhere [34]. By the end of the process, the viscous blue gels were dried at 350 °C for 2 h, then ground to fine powders and calcined at 900 °C for 10 h. These calcined powders were pressed using the uniaxial compression at a pressure of 150 MPa into pellets of approximately4.75 mm in radius and ~ 1.2 mm in thickness. To obtain $CaCu_{3-x}Mg_xTi_{4.2}O_{12}$ (x = 0.00, 0.05 and 0.10) ceramics, these pellets were separated for sintering at the same temperature of 1100 °C for 8 h and the others for 12 h. Effect of sintering time on the dielectric and non-ohmics properties, including the temperature stability of ε' were studied. The obtained ceramic samples $CaCu_{3-x}Mg_xTi_{4.2}O_{12}$ sintered at 1100 °C for 8 h with different Mg concentrations are denoted as Ti02/8, Ti02–Mg05/8 and Ti02–Mg10/8 for x = 0.00, 0.05 and 0.10, respectively. Similarly, for those samples sintered at 1100 °C for 12 h, Ti02/12, Ti02–Mg05/12 and Ti02–Mg10/12 symbols are denoted for them with x = 0.00, 0.05 and 0.10, respectively.

Structural and phase composition of ceramic samples were investigated by X-ray diffraction (PW3040 Philips; Cu-Kα radiation; λ = 0.15406 nm). Microstructure and the dispersion of Mg, Ca, Cu, Ti and O elements in ceramic samples were studied by field emission scanning electron microscope (FESEM) coupled with energy dispersive X-ray spectroscopy (EDXS) (LEO SEM VP1450, UK). Prior to the measurements of dielectric constant (ε') and dielectric loss tangent (tanδ) of ceramic samples, both surfaces of each sample were polished, subsequently cleaned and coated with Au using a Polaron SC500 sputtering unit. The measurements of dielectric constant (ε') and tanδ of ceramic samples

were performed in wide temperature (− 50 to 210 °C) and frequency (100 Hz–1 MHz) ranges using an impedance gain phase analyzer (Hewlett Packard Model 4294A). Nonlinear characteristics of ceramic samples were studied at RT using a high voltage measurement unit (Keithley Model 247). Nonlinear coefficients (α) were calculated by Eq. (1) and breakdown electric field (E_b) were determined at a current density (J) of 1 mA/cm^2.

$$\alpha = \frac{\log(J_2/J_1)}{\log(E_2/E_1)} \quad (1)$$

where E_1 and E_2 are the electric fields, corresponding to $J_1 = 1$ mA/cm^2 and $J_2 = 10$ mA/cm^2, respectively.

3 Results and discussion

Rietveld refinement profile fits for the XRD patterns of Ti02/8, Ti02–Mg05/8 and Ti02–Mg10/8 ceramics are shown in Fig. 1a–c and those of Ti02/12, Ti02–Mg05/12

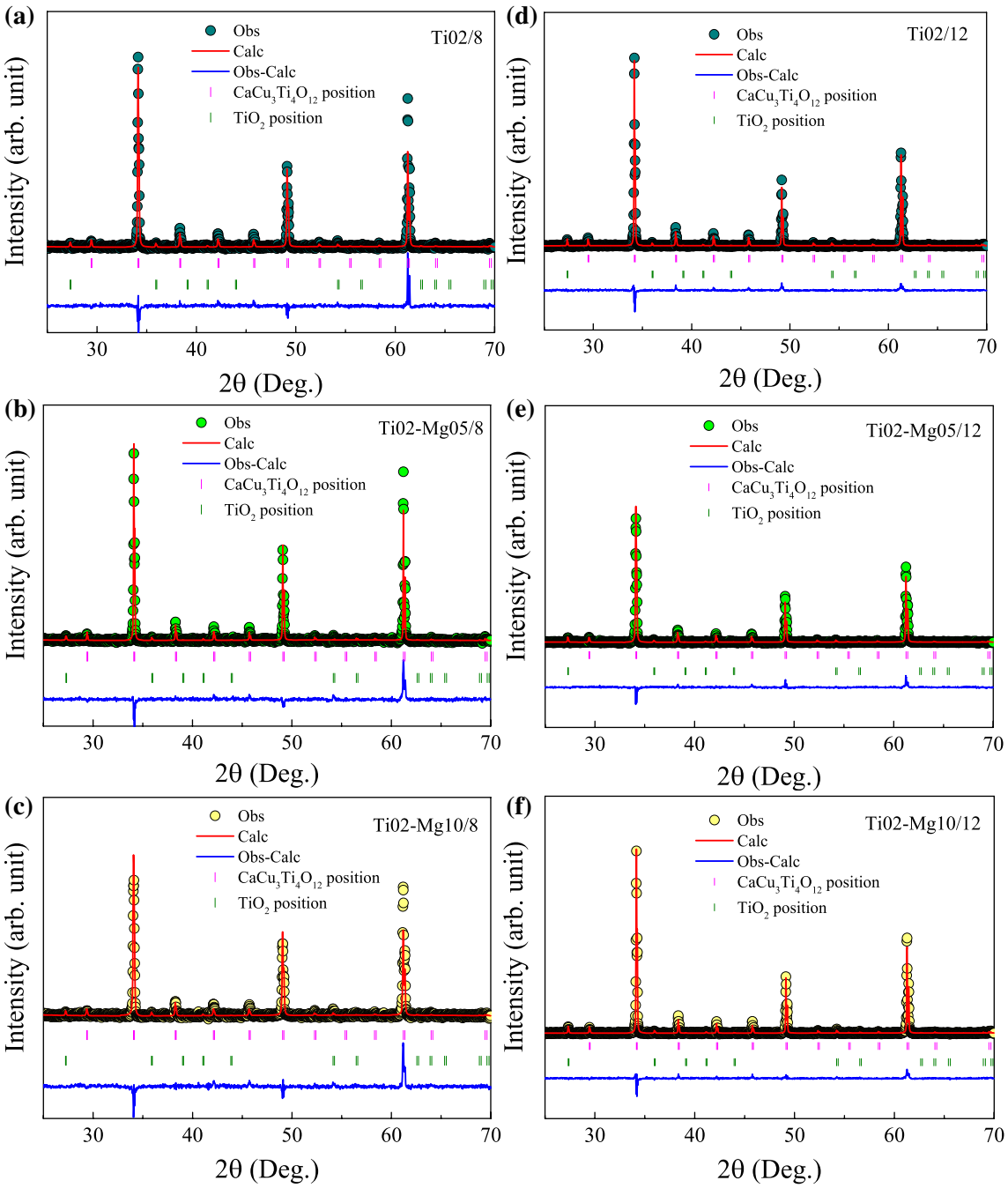

Fig. 1 Rietveld refinement fitting profiles of Ti02, Ti02–Mg05 and Ti02–Mg10 ceramics sintered at 1100 °C **a–c** for 8 h and **d–f** for 12 h

and Ti02–Mg10/12 ceramics are shown in Fig. 1d–f, respectively. As seen in Fig. 1a–f the profile fits for the main peaks of all ceramics correspond to those of the standard $CaCu_3Ti_4O_{12}$ (ICSD card No. 95714) with the detection of a minor diffraction peak of TiO_2 secondary phase (ICSD card No. 26715) in all ceramics. From Rietveld refinement fitting profiles the $CaCu_3Ti_4O_{12}$:TiO_2 ratios were determined from the main diffraction peaks of each $CaCu_{3-x}Mg_xTi_{4.2}O_{12}$ ceramic and found to have the same value of approximately 94:6. In addition, these main diffraction peaks in each of the XRD pattern can be perfectly indexed based on the *bcc* structure of a space group *Im3* (204). Complete details for the analysis of various R (R_{exp}, R_{wp}, and R_p) values and goodness of fit (*GOF*) were given elsewhere [35]. From Rietveld refinement results, *GOF* values are found to be in a narrow range of approximately 1.0–1.4 for all ceramics. The percentages of R (R_{exp}, R_{wp}, and R_p) factors for all ceramics are in the appropriate range of approximately 5–10%. Lattice parameters (a) of Ti02/8, Ti02–Mg05/8, Ti02–Mg10/8, Ti02/12, Ti02–Mg05/12 and Ti02–Mg10/12 ceramics were determined and found to be 7.387 (2), 7.388 (2), 7.386 (3), 7.389 (8), 7.388 (1) and 7.390 (8) Å, respectively. It is obvious that the lattice parameters (a) display no significant change with increasing Mg^{2+} concentration. This confirms the substitution of Mg^{2+} ion on the Cu site rather than the Ca site (having Ca^{2+} ion of large ionic radius 1.00 Å) due to the nearly equal ionic radius of Cu^{2+} (0.73 Å) and Mg^{2+} (0.72 Å). Moreover, the obtained a values of all ceramics are comparable with those of CCTO ceramics ($a = 7.391$ Å) reported in literatures [21]. According to the Rietveld refinement fitting profile results, the theoretical densities (D_{xrd}) of Ti02/8, Ti02–Mg05/8, Ti02–Mg10/8, Ti02/12, Ti02–Mg05/12 and Ti02–Mg10/12 ceramics were determined and found to be 5.0591, 5.0574, 5.0608, 5.0586, 5.0555 and 5.0534 g cm^{-3}, respectively. It is remarkable that D_{xrd} values of all $CaCu_{3-x}Mg_xTi_{4.2}O_{12}$ (Ti02–Mg) ceramics are less than that of $CaCu_3Ti_{4.2}O_{12}$ (Ti02) ceramic due to the lighter atomic mass of Mg atom (24.304 amu) than that of Cu atom (63.546 amu).

Since ε' and tanδ values with nonlinear J–E properties of CCTO ceramics are strongly dependent on their microstructure as generally reported in literatures [36]. Thus, morphology and microstructure of all ceramic samples were examined. As shown in Fig. 2a–f, are back scattered FESEM images of polished surface of $CaCu_{3-x}Mg_xTi_{4.2}O_{12}$ ceramics sintered at 1100 °C for 8 h and 12 h, respectively. These FESEM images reveal the microstructural evolution of grains in all ceramic samples as a result of sintering process. The mean grain sizes of Ti02/8, Ti02–Mg05/8, Ti02–Mg10/8, Ti02/12, Ti02–Mg05/12 and Ti02–Mg10/12 ceramics were found to be 8.433 ± 1.321, 5.343 ± 1.069, 7.016 ± 2.111, 8.446 ± 1.756, 6.626 ± 1.677 and 7.348 ± 1.571 µm, respectively. It is obvious that the mean grain sizes of Mg-doped ceramic samples sintered with different sintering time of 8 and 12 h slightly decrease, comparing with their undoped counterparts. This might result from the solute drag mechanism due to the substitution of Mg^{2+} ion of lighter atomic mass and smaller atomic radius, compare with those of Cu^{2+} ion, into the nominal composition of $CaCu_{3-x}Mg_xTi_{4.2}O_{12}$ ceramics. Slight change of the mean grain sizes is suggested to originate from the less difference in ionic radii of Mg^{2+} (0.72 Å) dopant and Cu^{2+} (0.73 Å) host ions. Furthermore, effect of sintering time can result in a slight increase of the mean grain sizes of all ceramics.

To observe the segregation of Mg^{2+} ions in the microstructure of all $CaCu_{3-x}Mg_xTi_{4.2}O_{12}$ ($x = 0.00$, 0.05 and 0.10) ceramics sintered at 1100 °C for 8 and 12 h, the EDXS spectra obtained at grain and GB with back scattered FESEM images of each sample were examined. For illustration, back scattered FESEM image of Ti02–Mg10/8 ceramic is shown in Fig. 3a with a marked point (1) for grain and point (2) for GB. However, EDXS spectra of all ceramic samples are not shown. The EDXS results indicate that Mg^{2+} ions can segregate at grains and GBs with preference to be at GB. The Ca:Cu:Ti:Mg:O ratios at grain (1) and GB (2) of Ti02–Mg10/8 ceramic were determined and found to be 6.30:32.76:0.45:32.72:27.78 At.% and 6.80:3 0.56:0.00:33.28:29.36 At.%, respectively. The determined Ca:Cu:Ti:Mg:O ratios at grain and GB for other ceramic samples are listed in Table 1. In addition, sintering time significantly affect the distribution of Mg^{2+} in grains and GBs as can be seen in Table 1 that Mg^{2+} ion in Ti02–Mg10/12 ceramic can be detected at both of grain and GB regions, whereas that of Ti02–Mg10/8 ceramic can be only detected at grain regions. This result is similar to that reported in literature [4]. The dispersion of each Ca, Cu, Ti, Mg and O element in all $CaCu_{3-x}Mg_xTi_{4.2}O_{12}$ ceramics were determined and observed by elements mapping using FESEM. As shown in Fig. 3b–f are the back scattered FESEM mapping images of Ca, Cu, Ti, Mg and O elements in Ti02–Mg10/8 ceramic, corresponding to its back scattered FESEM image shown in Fig. 3a. These results confirm the existence of all major elements of Ca, Cu, Ti, Mg and O with homogeneous dispersion of them in grains and GBs. It is obviously seen in Fig. 3e that segregation of Mg^{2+} dopant in any specific region of the ceramic is not observed.

The frequency dependence of ε' and tanδ for Ti02/8, Ti02–Mg05/8 and Ti02–Mg10/8 ceramics are shown in Fig. 4a and its inset. The determined ε' values (at 30 °C and 1 kHz) of Ti02/8, Ti02–Mg05/8 and Ti02–Mg10/8 ceramics were found to be 46,434, 12,902 and 14,012, respectively. These ε' values are summarized in Table 2. Notably, ε' value of Ti02–Mg05/8 ceramic decreases by a factor of approximately four times compare with that of undoped Ti02/8 ceramic. However, for further increasing Mg-doping content, ε' of Ti02–Mg10/8 ceramic slightly increase to a

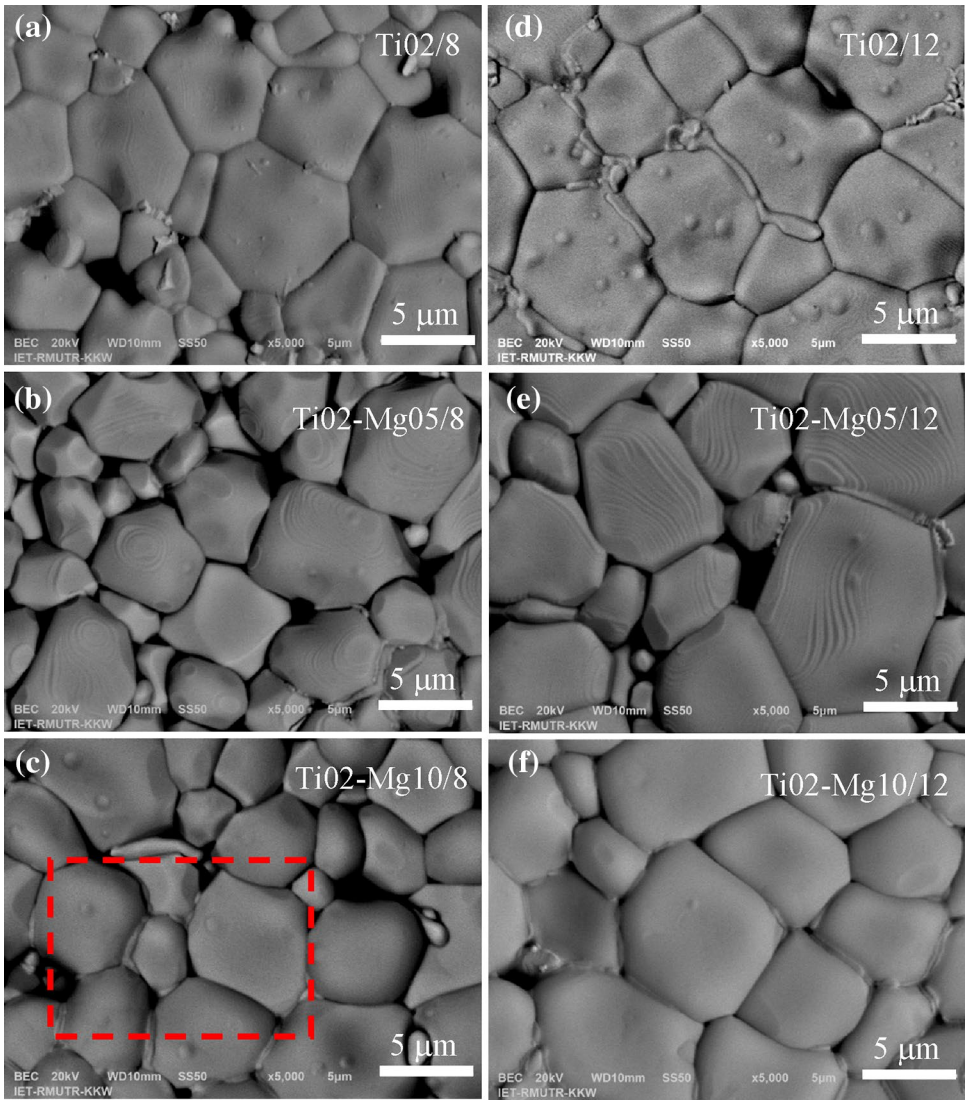

Fig. 2 Back scattered FESEM images of Ti02, Ti02–Mg05 and Ti02–Mg10 ceramics sintered at 1100 °C **a–c** for 8 h and **d–f** for 12 h

value, which is higher than that of Ti02–Mg05/8 ceramic. It is obvious that the ε' value of Mg^{2+}-doped Ti02 ceramic is lower than that of undoped Ti02 ceramic due to the lower concentration of oxygen vacancy at grain boundary (GB), which is consistent with those reported in literature [37–41]. In addition, Han et al. reported that free charge carrier at GB could play an important role on the improvement of dielectric properties of Y-doped CCTO ceramics [39]. Moreover, the ε' values of Mg-doped Ti02/8 ceramics are almost stable over a wide frequency range from 100 Hz to 1 MHz, while that of undoped Ti02/8 ceramic greatly decrease with increasing frequency. It is also remarkable that ε' values of Ti02–Mg05/8 and Ti02–Mg10/8 ceramics are approximately 3.5 and 3.3 times lower than that of undoped Ti02/8 ceramic. However, these ε' values are still large enough (higher than 10^4 at 30 °C and 1 kHz) and sufficient for capacitor application. In addition to high ε' value, tanδ value of high performance capacitor should be less than 0.05. As shown in the inset of Fig. 4a, the red dashed line signifies tanδ value equal to 0.05. At 30 °C and 1 kHz, tanδ values of Ti02/8, Ti02–Mg05/8 and Ti02–Mg10/8 ceramics are found to be 0.685, 0.011 and 0.009, respectively. These tanδ values are summarized in Table 2. It is obvious that tanδ values of Ti02–Mg05/8 and Ti02–Mg10/8 ceramics are smaller than 0.05 and both values are approximately 30 times less than that of Ti02/8 ceramic in a wide frequency range of 100 Hz–0.1 MHz. Figure 4b and its inset show the frequency dependence of ε' and tanδ of Ti02/12, Ti02–Mg05/12 and Ti02–Mg10/12 ceramics. At 30 °C and 1 kHz, ε' and tanδ values are found to be 199,083, 18,000 and 11,086; and 0.823, 0.014 and 0.009 for Ti02/12, Ti02–Mg05/12 and Ti02–Mg10/12 ceramics, respectively. All of these ε' and tanδ values are summarized in Table 2. It is interesting that tanδ values of the Ti02–Mg05/12 and Ti02–Mg10/12 ceramics are about 58 and 91 times less than that of undoped Ti02/12 ceramic, while the ε' values

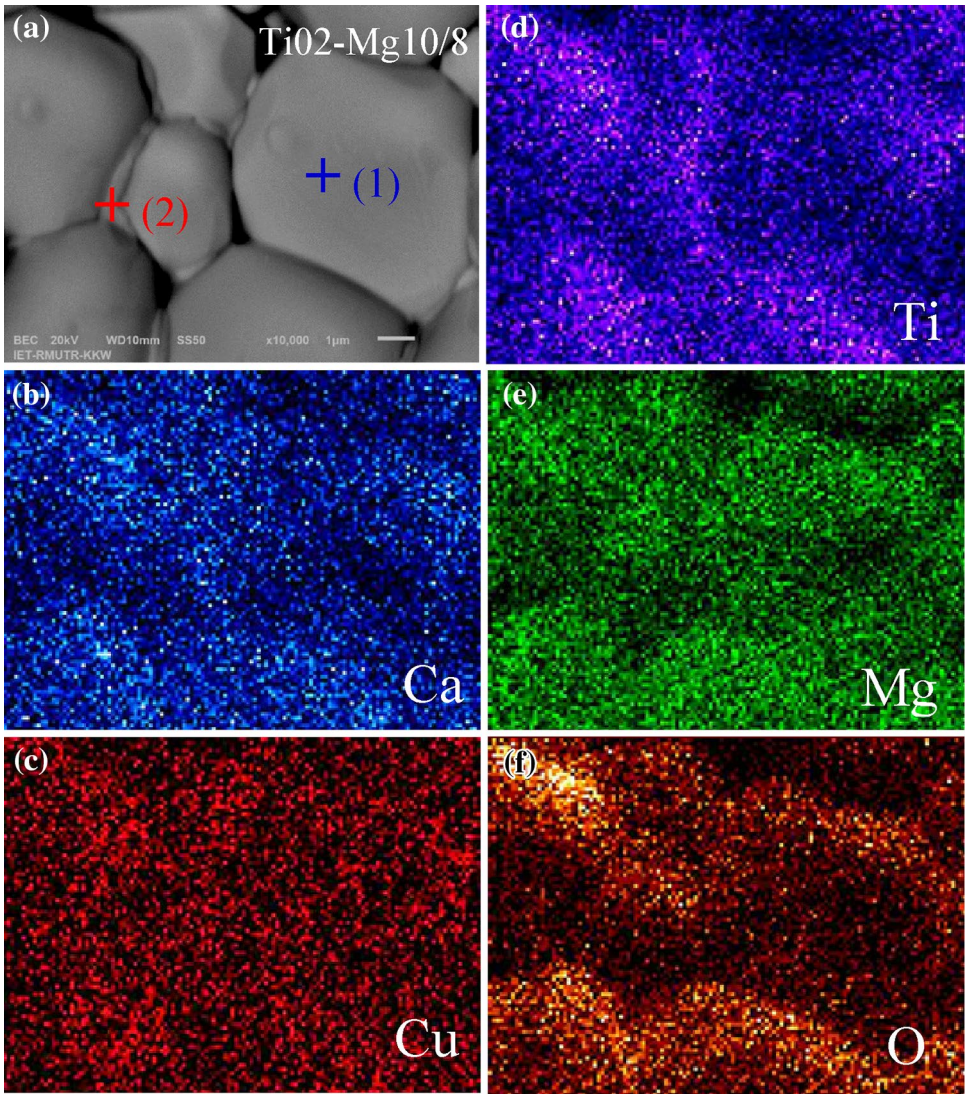

Fig. 3 **a** Back scattered FESEM image of Ti02–Mg10/8 ceramic, showing marked points (1) and (2) for grain and GB, respectively. **b–f** Element mapping of Ca, Cu, Ti, Mg and O corresponding to back scattered FESEM image in **a**

Table 1 Ca:Cu:Mg:Ti:O atomic ratios obtained from the EDXS results at selected point (1) large grain and (2) GB in all $CaCu_{3-x}Mg_xTi_{4.2}O_{12}$ (x = 0.00, 0.05 and 0.10) ceramics sintered at 1100 °C for 8 and 12 h

Sample	Point	Ca (At.%)	Cu (At.%)	Mg (At.%)	Ti (At.%)	O (At.%)
1100 °C for 8 h						
Ti02/8	1	7.09	27.56	0.00	37.32	33.41
	2	5.42	21.51	0.00	26.27	46.51
Ti02–Mg05/8	1	7.03	27.59	0.58	31.27	33.52
	2	4.87	27.39	0.00	34.03	33.71
Ti02–Mg10/8	1	6.30	32.76	0.45	32.72	27.78
	2	6.80	30.56	0.00	33.28	29.36
1100 °C for 12 h						
Ti02/12	1	5.28	29.55	0.00	28.26	36.91
	2	6.05	20.87	0.00	23.58	49.00
Ti02–Mg05/12	1	6.57	27.56	1.18	31.23	33.45
	2	7.41	40.92	0.00	35.16	16.51
Ti02–Mg10/12	1	6.56	23.96	1.19	30.57	37.71
	2	6.60	23.42	0.58	29.33	40.08

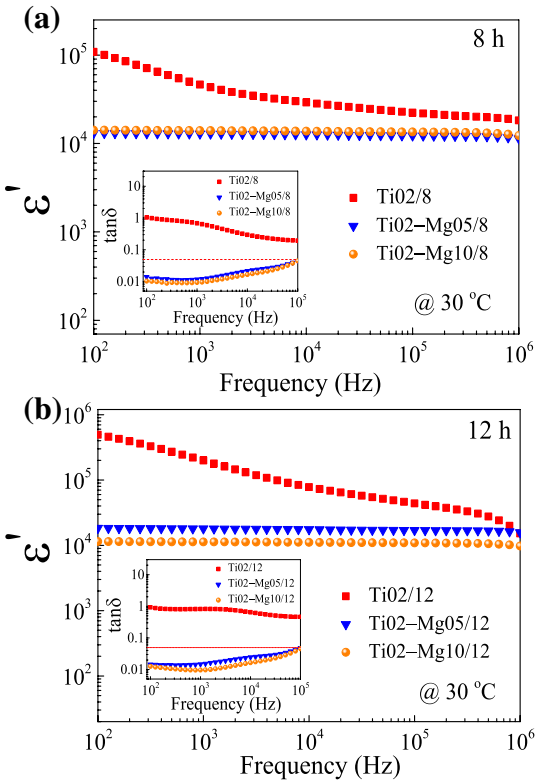

Fig. 4 Frequency dependence of ε' and tanδ (inset) of Ti02, Ti02–Mg05 and Ti02–Mg10 ceramics sintered at 1100 °C **a** for 8 h and **b** for 12 h

of them are approximately 11 and 18 times less than that of undoped Ti02/12 ceramic. It worth noting that increasing sintering time from 8 to 12 h, tanδ value of undoped Ti02 ceramic greatly increase, whereas those of Ti02–Mg05 and Ti02–Mg10 ceramics slightly increase to a stable value. Moreover, ε' values of Ti02 and Ti02–Mg05 ceramics are greatly increase with increasing sintering time from 8 to 12 h, whereas that of Ti02–Mg10 ceramic slightly decrease. It is obvious that the increase of sintering time at the sintering temperature of 1100 °C can greatly promote oxygen vacancy and Ti^{3+}, which play an important role on the improvement of electrical properties of these samples in consistent with those reported in literature [16, 42, 43]. Notably, the very low tanδ (~ 0.009 to 0.014) and giant ε' (~ 11,086 to 18,000) values of the Mg-doped Ti02 ceramics are comparable with those reported in literatures [44–46]. Furthermore, the lowest tanδ value of 0.009 (at RT and 1 kHz) is achieved in both Ti02–Mg10/8 and Ti02–Mg10/12 ceramics. This tanδ value is approximately 1.4, 1.6, 4.0 and 4.3 times less than those obtained in (Y + Mg) co-doped CCTO [5], $Ca_2Cu_{3-x}Mg_xTi_4O_{12}$ [4], $Na_{1/2}Y_{1/2}Cu_{3-x}Mg_xTi_4O_{12}$ [47] and ($Sm^{3+}$and Mg^{2+}) co-doped CCTO [32] ceramics, respectively. It is notable that, all Mg-doped Ti02 ceramics sintered for 8 and 12 h demonstrate giant ε' and very low tanδ values. Thus, it can be concluded that all Mg-doped Ti02 ceramics demonstrate very low tanδ and high ε' over a wide frequency range, which is appropriate for capacitor application.

The temperature dependence of ε' at 1 kHz for all ceramic samples sintered at 1100 °C for 8 and 12 h are shown in Fig. 5a, b, respectively. As seen in Fig. 5a, b, ε' values of undoped Ti02/8 and Ti02/12 ceramics greatly increase with increasing temperature, whereas those of Mg-doped Ti02 ceramics are almost stable in a temperature range of − 60 to 210 °C. The greatly temperature dependence of ε' in undoped Ti02 ceramics is similar to that observed in CCTO ceramics [53, 54]. Figure 5c, d display the temperature dependence of tanδ at 1 kHz for all ceramic samples sintered at 1100 °C for 8 and 12 h, respectively. It is obvious in Fig. 5c, d that when the temperature is higher than 100 °C, tanδ of all Mg-doped Ti02 ceramics is higher than 0.05. In addition, tanδ values of both undoped Ti02 ceramics are higher than 0.05 through the whole temperature range from − 50 to 210 °C. The large increase in tan δ at high temperatures of both undoped Ti02 ceramics is consistent with their great increase in ε'. It is likely that the large value of tanδ in a high temperature region is the most serious problem one that limit the potent application of CCTO-based compounds at high temperature. Therefore, it is evident that Mg doping in Ti02 ceramics can result not only in the temperature stability of ε', but also simultaneously improve temperature stability of tanδ.

As shown in Fig. 5e, f are the $\Delta\varepsilon'$ values of ceramic samples sintered at 1100 °C for 8 and 12 h, respectively. All of these values are evaluated at the frequency of 1 kHz from the following equation,

$$\Delta\varepsilon' = 100 \times \frac{\varepsilon'_T - \varepsilon'_{30}}{\varepsilon'_{30}}\ (\%), \tag{2}$$

where ε'_T and ε'_{30} are ε' at a temperature of T and 30 °C, respectively. In addition to high ε' and low tanδ, a good capacitor should have $\Delta\varepsilon' < \pm 15\%$ over a wide temperature range. As seen in Fig. 5e, f, $\Delta\varepsilon'$ of both undoped Ti02 ceramics abruptly change in a very narrow temperature range of 10 °C. In contrast to this, $\Delta\varepsilon' < \pm 15\%$ of both Mg-doped Ti02 ceramics sintered for 8 h, as shown in Fig. 5e, are found to slowly vary in a more wider temperature range of − 60 to 170 °C and − 60 to 210 °C for Ti02–Mg05/8 and Ti02–Mg10/8, respectively. Similar behavior of $\Delta\varepsilon' < \pm 15\%$ is observed in Ti02–Mg05/12 and Ti02–Mg10/12 ceramics, as shown in Fig. 5f with temperature stability in a range of − 60 to 180 °C and − 60 to 210 °C, respectively. It worth noting that dielectric properties of both Ti02–Mg05/8 and Ti02–Mg05/12 ceramics satisfy the EIA X5R, X7R and X8R standard capacitor specification. Interestingly, Ti02–Mg10/8 and Ti02–Mg10/12 ceramics satisfy the EIA X5R, X7R, X8R and X9R standard capacitors. In addition to the

Table 2 Comparison of dielectric constant (ε') and loss tangent (tanδ) at RT and 1 kHz, R_g and R_{gb} values at 120 °C, temperature range (ΔT) for $\Delta\varepsilon' < \pm 15\%$, α and E_b values at RT, barrier heights (φ_B), and potential barrier width (β) for all $CaCu_{3-x}Mg_xTi_{4.2}O_{12}$ (x = 0.00, 0.05 and 0.10) ceramics sintered at 1100 °C for 8 and 12 h in this work with those reported in other capacitor materials

Sample	Sintering conditions	ε' (RT)	tanδ (RT)	*Rg* (Ω cm)	*Rgb* (Ω cm)	ΔT (°C)	α	*Eb* (V cm−1)	φB (eV)	β (V−1/2 cm1/2)
Ti02/8[a]	1100 °C/8 h	46,434	0.685	25	3310	–	2.70	422.75	0.727	0.0069
Ti02–Mg05/8[a]	1100 °C/8 h	12,902	0.011	59	1,030,000	−60 to 170	13.75	5756.24	0.963	0.0058
Ti02–Mg10/8[a]	1100 °C/8 h	14,012	0.009	45	1,750,000	−60 to 210	13.64	5977.02	0.970	0.0059
Ti02/12[a]	1100 °C/12 h	199,083	0.823	82	1369	–	1.78	85.54	0.649	0.0068
Ti02–Mg05/12[a]	1100 °C/12 h	18,000	0.014	27	1,600,000	−60 to 180	13.48	4688.25	0.957	0.0063
Ti02–Mg10/12[a]	1100 °C/12 h	11,086	0.009	34	2,530,000	−60 to 210	13.59	5808.11	0.966	0.0059
$CaCu_3Ti_{3.98}Y_{0.02}O_{12}$ [48]	1080 °C/12 h	32,000	~0.800	1228^{RT}	4647^{RT}	–	–	–	–	–
BNT-0.03Yb($(Bi_{0.5}Na_{0.5})_{0.97}Yb_{0.03}TiO_3$) [49]	1200 °C /2 h	~1204	~0.038[c]	–	–	147 to 528[b]	–	–	–	–
BB30La (0.4($Ba_{0.8}Ca_{0.2})_{0.7}La_{0.3}TiO_3$-0.6Bi($Mg_{0.5}Ti_{0.5}$)$O_3$) [50]	1350 °C /4 h	~700	~0.064[c]	–	–	30 to 550[b]	–	–	–	–
BLZT-3($Ba_{0.94}La_{0.06}(Zr_{0.9}Ti_{0.1})_{0.985}O_3$) [43]	1380 °C /4 h	$\sim 400^{577\,c}$	$\sim 0.25^{577\,c}$	–	$\sim 650000^{577\,c}$	–	–	–	–	–
$CaCu_3Ti_4O_{12}$ [51]	1040 °C/30 h	~700 [c]	~0.030 [c]	68^{25}	5500000^{25}	–	–	–	–	–
$CaCu_{2.7}Ti_4O_{12}$ [52]	1060 °C/48 h	~20,000[c]	–	49.9^{25}	$>100000^{25}$	–	–	–	–	–

[a]In this work, 25 = at 25 °C, 577 = at 577 °C

[b]$\Delta\varepsilon' < \pm 10\%$

[c]Estimated numerical values from figures in cited references

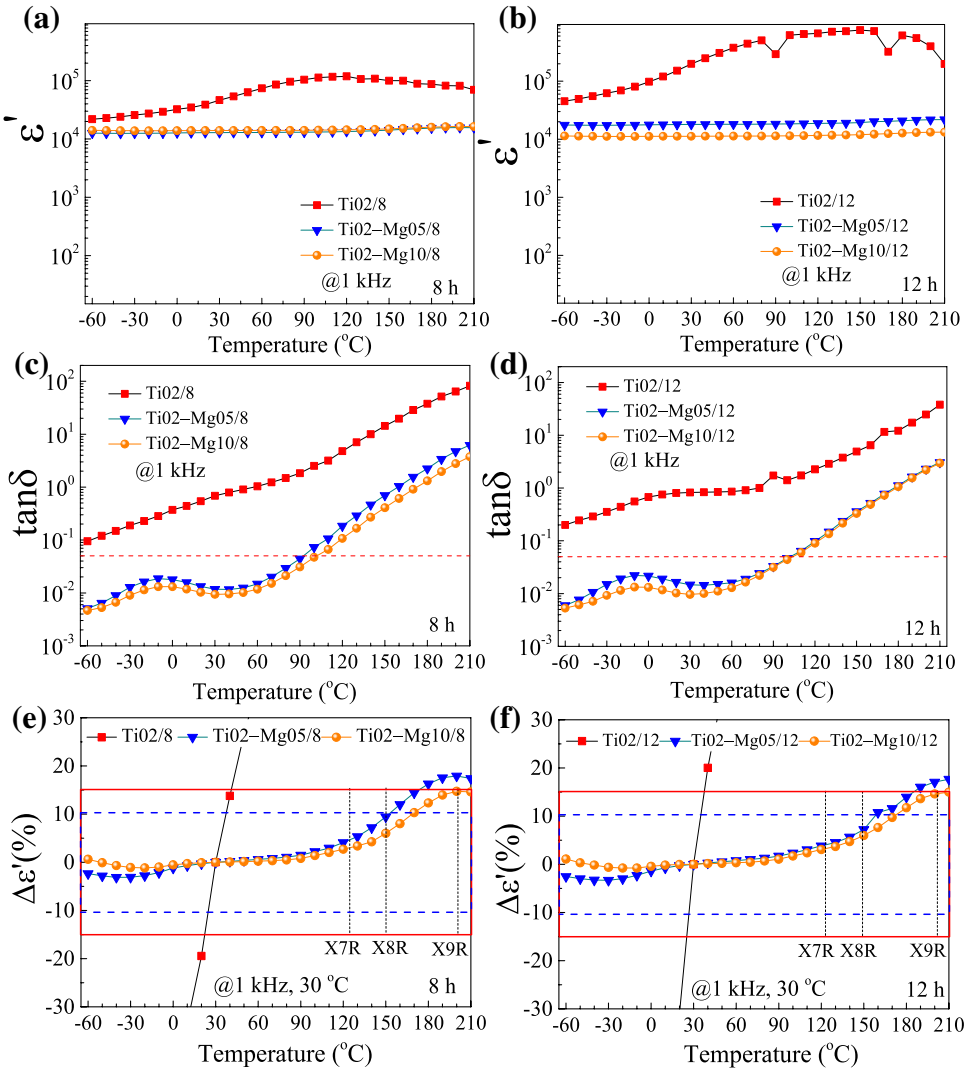

Fig. 5 Temperature dependence of ε' (**a** and **b**), tanδ (**c** and **d**) and $\Delta\varepsilon'$ (**e** and **f**) for Ti02, Ti02–Mg05 and Ti02–Mg10 ceramic samples. **a, c** and **e** sintered for 8 h. **b, d** and **f** sintered for 12 h

application for X–R capacitors, all Mg-doped Ti02 ceramics have a potent use for other EIA code X–P capacitors, which is defined with the temperature stability condition that $\Delta\varepsilon' < \pm 10\%$ should be in a temperature range of -55 to 125 °C and -55 to 150 °C for the EIA code X7P and X8P capacitors, respectively. In Fig. 5e, f, the blue dashed lines are drawn to signify $\Delta\varepsilon' < \pm 10\%$. As illustrated in Fig. 5e, it is clear that $\Delta\varepsilon' < \pm 10\%$ for Ti02–Mg05/8 and Ti02–Mg10/8 are in temperature ranges of -60 to 150 °C and -60 to 170 °C, respectively. Similarly, these temperature ranges of $\Delta\varepsilon' < \pm 10\%$ are found to be -60 to 160 °C and -60 to 170 °C for Ti02–Mg05/12 and Ti02–Mg10/12 ceramics, respectively. Therefore, it can be concluded that, Ti02–Mg05 and Ti02–Mg10 ceramics sintered for 8 and 12 h not only satisfy for the EIA code X–R capacitors, but also beneficial for the EIA code X–P capacitors. Furthermore, the temperature stability of Ti02–Mg05 ceramics also slightly increases with the increasing sintering time from 8 to 12 h. Notably, the achievement of excellent dielectric properties and a wide range temperature stability of ε' in Mg-doped TiO_2 ceramics are difficult to attain in other CCTO-based giant dielectric materials.

In this work, although the $\Delta\varepsilon' < \pm 15\%$ of Mg-doped Ti02 ceramics is stable in a temperature range comparable to those of other co-doped CCTO ceramics [5, 32], its performance of temperature stability is better than those reported in a binary system of $Ca_2Cu_{2-x}Mg_xTi_4O_{12}$ ceramics [4] and other Mg-doped $CaCuTi_4O_{12}$ ceramics [44–46]. Thus, it is verified that Mg-doped $CaCu_3Ti_{4.2}O_{12}$ ceramics prepared by the PP method can be successfully modified and categorized for the EIA code X9R capacitors. In this work, it is evident and can be concluded that dielectric properties, high ε' and low tanδ with the excellent temperature coefficient $\Delta\varepsilon'$, of Ti02 ceramics can be significantly improved by Mg^{2+} doping, follow with a proper sintering process treatment.

The nonlinear *J–E* properties of all ceramic samples were examined at RT. As shown in Fig. 6a, b are nonlinear *J–E* characteristic curves of Mg-doped $CaCu_3Ti_{4.2}O_{12}$ ceramic

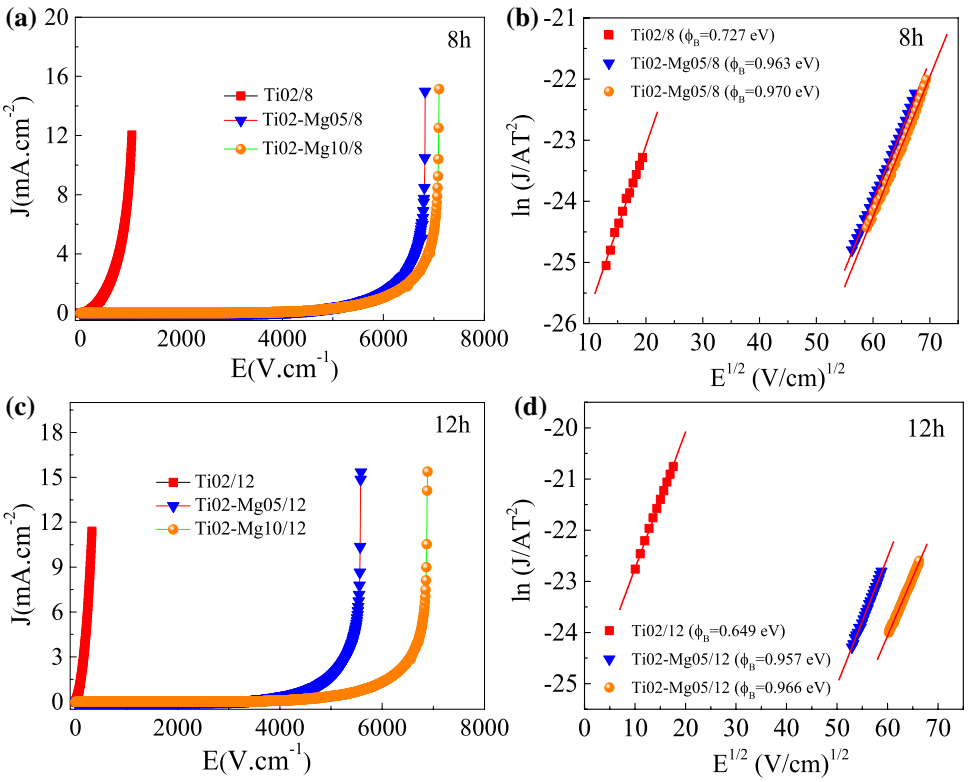

Fig. 6 **a, b** and **c, d** display *J–E* curves at RT and plots of *ln* (J/AT^2) versus E$^{1/2}$ for ceramic samples sintered at 1100 °C for 8 and 12 h, respectively

samples sintered at 1100 °C for 8 and 12 h, respectively. Nonlinear coefficient (α) and breakdown field (E_b) of all prepared ceramics can be determined from these *J–E* curves. The obtained α and E_b values of Ti02, Ti02–Mg05 and Ti02–Mg10 ceramics are summarized in Table 2. It worth noting that α and E_b values of Mg-doped Ti02 ceramics significantly increase with increasing Mg^{2+} doping content. In addition, both α and E_b values are reduced by increasing sintering time. It is suggested that the enhancement of α and E_b values might arise from the immense increase of R_{gb} [14, 55]. It is remarkable in Table 2 that the maximum E_b values observed in Ti02–Mg10/8 and Ti02–Mg10/12 ceramics are closely correlated with the highest values of R_{gb} and the lowest tanδ values with very high thermal stability of ε'. The values of α and E_b are comparable with those reported in literatures [13, 22, 24, 56]. Furthermore, the α values obtained in this work are higher than those of 5.1–7.9 reported for $CaCu_3Ti_{4+x}O_{12+2x}$ ($0.00 < x < 1.5$) ceramics sintered at 1100 °C for 3 h [27]. In order to understand the electrical respond at GBs of these ceramic samples, the potential barriers are discussed based on Schottky barrier [57]. Based on this type of barrier, the electrical current density (J) and the applied electrical field (E) are related by the relationship, $\ln\left(J/AT^2\right) = \frac{1}{k_BT}\left(\beta E^{1/2} - \phi_B\right)$ [58, 59], where A is the Richardson constant ($\sim 1202 \times 10^2$ mA cm^{-2} K^{-2}), k_B is the Boltzmann constant (1.3806×10^{-23} m^2 kg s^{-2} K^{-1}), β is a constant related to the potential barrier width, and φ_B is the barrier high. As seen in Fig. 6c, d a good linear relationship of *ln* (J/AT^2) versus E$^{1/2}$ is obtained for ceramic samples sintered at 1100 °C for 8 and 12 h. From the fitting results, the φ_B and β values of all ceramic samples are obtained and summarized in Table 2. It is also found that the φ_B value of Ti02 ceramic is greatly increased with Mg^{2+} doping. It is suggested that the formation of the electrostatic potential barriers at GBs is due to the present of Mg^{2+} ions. Moreover, the α and E_b values are directly promotional to the φ_B and 1/β values, respectively. In addition, it is suggested that reducing of the β value can increase the E_b value, whereas the α is improved by the increasing of φ_B values. Notably, φ_B values (0.957–0.970 eV) of these Mg^{2+}-doped Ti02 ceramics are comparable with the φ_B values of the $Na_{1/2}Sm_{1/2}Cu_3Ti_4O_{12}$ ceramics (~0.964 eV) [60].

In order to further study the effect of Mg^{2+} doping on the resistance of grain (R_g) and grain boundary (R_{gb}), the Z^* plots at 120 °C of all ceramic samples were performed as shown in Fig. 7a. Generally, the semicircular arcs at low and high frequency ranges in Z^* plots correspond to R_{gb} and R_g, respectively [12, 61]. As seen in Fig. 7a for illustration, only the low frequency semicircular arcs are observed in Ti02/8, Ti02–Mg05/8 and Ti02–Mg10/8 ceramic samples. This behavior is similar to those of ceramic samples sintered for 12 h. In Fig. 7a and the inset (1), R_{gb} values of Ti02/8, Ti02–Mg05/8 and Ti02–Mg10/8 ceramics were estimated and found to be 3310, 1,030,000 and

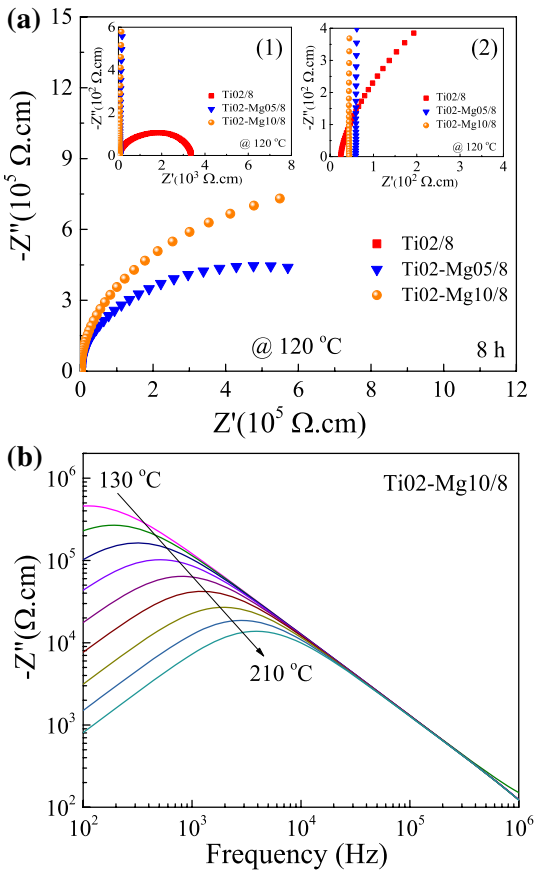

Fig. 7 **a** Impedance complex plane plots (Z^*) at 120 °C of Ti02/8, Ti02–Mg05/8 and Ti02–Mg10/8 ceramics with inset (1) displays a magnification of the overlapped region and (2) displays an expanded view of high frequency data close to the origin. **b** Frequency dependence of $-Z''$ in the temperature range of 130–210 °C for Ti02–Mg10/8 ceramic

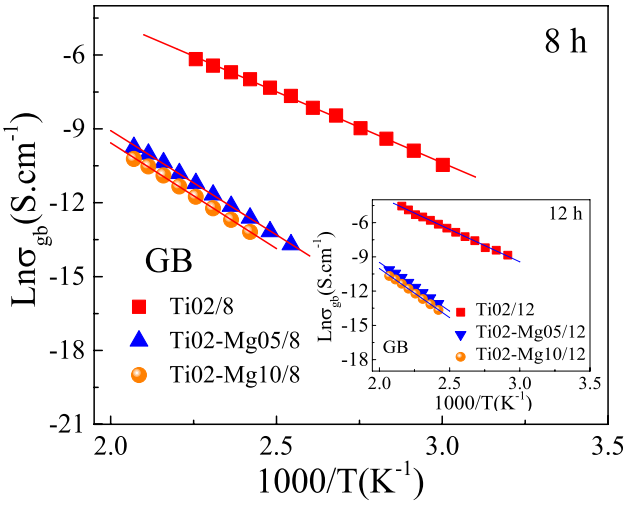

Fig. 8 Arrhenius plots of $\ln\sigma_{gb}$ for the Ti02, Ti02–Mg05 and Ti02–Mg10 ceramics sintered at 1100 °C for 8 h with inset displays the same plots of ln σ_{gb} for these ceramics sintered for 12 h

1,750,000 Ω cm, respectively. These values are summarized in Table 2. As seen in the inset (2) of Fig. 7a, R_g values of Ti02/8, Ti02–Mg05/8 and Ti02–Mg10/8 ceramics are estimated from a nonzero intercept on the Z' axis at high frequency region and found to be 25, 59 and 45 Ω cm, respectively. Similarly, R_{gb} and R_g values at 120 °C of Ti02/12, Ti02–Mg05/12 and Ti02–Mg10/12 ceramics were also estimated and summarized in Table 2. It is notable in Table 2 that R_{gb} values of Ti02/8 and Ti02/12 ceramics increase with increasing Mg^{2+} dopants, which is similar to those observed in literatures [5, 44, 47]. Furthermore, increasing sintering time from 8 h to 12 h can also increase R_{gb} values for Mg-doped Ti02 ceramic samples with the opposite decreasing of these values as observed in undoped Ti02 ceramic samples. Thus, it is obvious that sintering time can significantly influence on the total resistance of the insulating parts i.e. R_{gb} of ceramic samples, as well. This might primarily originate from the GBs and/or outer surface layers. In addition, R_{gb} is observed to relate with the very high temperature coefficient of ε' i.e. undoped Ti02 ceramic with low value of R_{gb} exhibits a poor temperature stability of ε', whereas Mg-doped Ti02 ceramic samples with high R_{gb} value demonstrate the excellent temperature stability of ε'. Therefore, Mg-doped Ti02 ceramic samples of high performance dielectric properties with the excellent temperature stability of ε' can be well described by their large R_{gb} values.

As shown in Fig. 8 and its inset are the temperature dependence of grain boundary conductivity (σ_{gb}) for ceramic samples sintered at 1100 °C for 8 and 12 h, respectively. As seen in Fig. 8, the plots follow the Arrhenius law,

$$\ln \sigma_{gb} = \left(\frac{-E_{gb}}{k_B T}\right) + \ln \sigma_0 \tag{3}$$

where the values of σ_{gb} is defined by $\sigma_{gb} = 1/R_{gb}$, σ_0 is the pre-exponential term, E_{gb} is the activation energy for conduction at grain boundaries, k_B is the Boltzmann constant, and T is the absolute temperature. E_{gb} values are generally calculated from the slopes of the plots of Ln σ_{gb} versus 1000/T and found to be 0.419, 0.611 and 0.623 eV for Ti02/8, Ti02–Mg05/8 and Ti02–Mg10/8 ceramics, respectively. As for Ti02/12, Ti02–Mg05/12 and Ti02–Mg10/12 ceramics, the E_{gb} values are found to be 0.413, 0.620 and 0.625 eV, respectively. It worth noting that, E_{gb} values of Ti02–Mg/8 and Ti02–Mg/12 ceramics increase with increasing Mg^{2+} doping concentration, which is consistent with the increase of their R_{gb} values, indicating the decrease of oxygen vacancy concentration at GB. All calculated E_{gb} values in this work are comparable with the conduction activation energy at GB of other CCTO ceramics ($E_{gb} \sim 0.47$–0.74 eV) [16, 42, 62] and Ln^{3+}-doped $CaCu_3Ti_4O_{12}$ ceramics ($E_{gb} \sim 0.55$–0.76 eV) [63].

Remarkably, the highest E_{gb} values are observed in both Ti02–Mg10/8 and Ti02–Mg10/12 ceramics, corresponding with the lowest tanδ values and the highest E_b values as revealed in Fig. 6a, b and the results summarized in Table 2. Consequently, it can be concluded that Mg^{2+} doping of Ti02 ceramics can result in a large increase of R_{gb}, E_b and E_{gb} values with the excellent temperature stability of ε' and very high performance of dielectric properties (giant ε' and very low tanδ).

4 Conclusion

Very high temperature stability of $\varepsilon' < \pm 15\%$ in a range of − 60–210 °C with giant ε' of 1.1×10^4–1.4×10^4 and very low tanδ of 0.009 are achieved in the $CaCu_{2.9}Mg_{0.1}Ti_{4.2}O_{12}$ ceramics sintered at 1100 °C for 8 and 12 h. Sintering time can immensely improve the ε' of $CaCu_3Ti_{4.2}O_{12}$ ceramic with increasing tanδ value, as well. Mg^{2+} doping of $CaCu_3Ti_{4.2}O_{12}$ ceramic results in the decrease of ε' value with very low tanδ value, consistent with the immense increase of GB resistance (R_{gb}). Longer sintering time can reduce the R_{gb} of $CaCu_3Ti_{4.2}O_{12}$ ceramic, but increase those of Mg-doped $CaCu_3Ti_{4.2}O_{12}$ ceramics. In addition, the nonlinear *J–E* properties of Mg-doped $CaCu_3Ti_{4.2}O_{12}$ ceramics (α and E_b values) significantly increase with increasing Mg^{2+} doping content, especially for the E_b value. Consequently, it can be concluded that excellent dielectric properties i.e. very high ε' and low tanδ with excellent temperature coefficient of $CaCu_3Ti_{4.2}O_{12}$ ceramics prepared in this work by the PP method can be significantly improved by Mg^{2+} doping follow with a proper sintering process treatment. This improvement can be explained by the enhancement of electrical responses at GBs resulting from the existence of Mg^{2+} ions. Moreover, it is suggested that $CaCu_{2.9}Mg_{0.1}Ti_{4.2}O_{12}$ ceramics sintered at 1100 °C for 8 and 12 h can be applicable for high temperature semiconductor devices such as X8R and X9R capacitors.

Acknowledgements This work was financially supported by the National Research Council of Thailand (NRCT) under Rajamangala University of Technology Rattanakosin (Grant No. 2562). It was also supported by the Thailand Research Fund through the Royal Golden Jubilee Ph.D. Program (PHD/0207/2558). The Nanotec-KKU Center of Excellence on Advanced Nanomaterials for Energy Production and Storage, Khon Kaen, Thailand and Integrated Nanotechnology Research Center (INRC), Department of Physics, Faculty of Science, Khon Kaen University, Khon Kaen, 40002 Thailand are also grateful for their co-financial support. The authors express their appreciation to the National Metal and Materials Technology Center (MTEC), Thailand Science Park, Pathumthani, Thailand for dielectric measurements.

References

1. S. Gao, S. Wu, Y. Zhang, H. Yang, X. Wang, Mater. Sci. Eng. B **176**, 68–71 (2011)
2. C. Sun, X. Wang, C. Ma, L. Li, J. Am. Ceram. Soc. **92**, 1613–1616 (2009)
3. Z. Hu, B. Cui, M. Li, L. Li, J. Mater. Sci.: Mater. Electron. **24**, 3850–3855 (2013)
4. J. Jumpatam, B. Putasaeng, T. Yamwong, P. Thongbai, S. Maensiri, J. Eur. Ceram. Soc. **34**, 2941–2950 (2014)
5. J. Boonlakhorn, B. Putasaeng, P. Kidkhunthod, P. Thongbai, Mater. Des. **92**, 494–498 (2016)
6. S.M. Galeb, H. Maher, U.S. Patent US6727200 B2 (2004)
7. B. Tang, S.-R. Zhang, X.-H. Zhou, Y. Yuan, L.-B. Yang, J. Electroceram. **25**, 93–97 (2010)
8. Z. Shen, X. Wang, L. Li, J. Mater. Sci.: Mater. Electron. **28**, 3768–3773 (2017)
9. X. Huang, W. Zhang, J. Xie, Q. Xu, L. Zhang, H. Hao, H. Liu, M. Cao, J. Mater. Sci.: Mater. Electron. **28**, 4204–4210 (2017)
10. C. Su, H. Hao, Q. Xu, Y. Lu, M. Appiah, C. Diao, M. Cao, Z. Yao, H. Liu, J. Mater. Sci.: Mater. Electron. **27**, 6140–6149 (2016)
11. Z. Liu, H. Fan, S. Lei, X. Ren, C. Long, J. Eur. Ceram. Soc. **37**, 115–122 (2017)
12. T.B. Adams, D.C. Sinclair, A.R. West, Phys. Rev. B **73**, 094124 (2006)
13. J. Boonlakhorn, P. Kidkhunthod, B. Putasaeng, T. Yamwong, P. Thongbai, S. Maensiri, J. Mater. Sci.: Mater. Electron. **26**, 2329–2337 (2015)
14. S.-Y. Chung, J.-H. Choi, J.-K. Choi, Appl. Phys. Lett. **91**, 091912 (2007)
15. J. Jumpatam, B. Putasaeng, T. Yamwong, P. Thongbai, S. Maensiri, Ceram. Int. **39**, 1057–1064 (2013)
16. Y. Huang, D. Shi, Y. Li, G. Li, Q. Wang, L. Liu, L. Fang, J. Mater. Sci.: Mater. Electron. **24**, 1994–1999 (2013)
17. Z. Kafi, A. Kompany, H. Arabi, A. Khorsand Zak, J. Alloys Compd. **727**, 168–176 (2017)
18. C. Long, T. Li, H. Fan, Y. Wu, L. Zhou, Y. Li, L. Xiao, Y. Li, J. Alloys Compd. **658**, 839–847 (2016)
19. G. Liu, H. Fan, J. Xu, Z. Liu, Y. Zhao, RSC Adv. **6**, 48708–48714 (2016)
20. X. Liu, H. Fan, J. Shi, Q. Li, Sci. Rep. **5**, 12699 (2015)
21. M.A. Subramanian, D. Li, N. Duan, B.A. Reisner, A.W. Sleight, J. Solid State Chem. **151**, 323–325 (2000)
22. P. Leret, J.F. Fernandez, J. de Frutos, D. Fernández-Hevia, J. Eur. Ceram. Soc. **27**, 3901–3905 (2007)
23. Z. Yang, L. Zhang, X. Chao, L. Xiong, J. Liu, J. Alloys Compd. **509**, 8716–8719 (2011)
24. J. Boonlakhorn, P. Kidkhunthod, B. Putasaeng, P. Thongbai, Ceram. Int. **43**, 2705–2711 (2017)
25. S. Vangchangyia, T. Yamwong, E. Swatsitang, P. Thongbai, S. Maensiri, Ceram. Int. **39**, 8133–8139 (2013)
26. J. Boonlakhorn, P. Kidkhunthod, P. Thongbai, S. Maensiri, Ceram. Int. **42**, 8467–8472 (2016)
27. Y.-H. Lin, J. Cai, M. Li, C.-W. Nan, J. He, Appl. Phys. Lett. **88**, 172902 (2006)
28. X. Ouyang, M. Habib, P. Cao, S. Wei, Z. Huang, W. Zhang, W. Gao, Ceram. Int. **41**, 13447–13454 (2015)
29. W. Hao, P. Xu, M. Wang, S. Yang, W. Yupeng, H. Wu, L. Sun, E. Cao, Y. Zhang, J. Alloys Compd. **740**, 1159–1164 (2018)
30. M. Li, G. Cai, D.F. Zhang, W.Y. Wang, W.J. Wang, X.L. Chen, J. Appl. Phys. **104**, 074107 (2008)
31. L. Ni, X.M. Chen, Solid State Commun. **149**, 379–383 (2009)
32. J. Boonlakhorn, P. Kidkhunthod, P. Thongbai, J. Eur. Ceram. Soc. **35**, 3521–3528 (2015)

33. P. Thongbai, B. Putasaeng, T. Yamwong, S. Maensiri, J. Alloys Compd. **509**, 7416–7420 (2011)
34. E. Swatsitang, A. Niyompan, T. Putjuso, J. Mater. Sci.: Mater. Electron. **24**, 3514–3520 (2013)
35. E. Jansen, W. Schäfer, G. Will, J. Appl. Crystallogr. **27**, 492–496 (1994)
36. J.-W. Lee, J.-H. Koh, Ceram. Int. **41**, 10442–10447 (2015)
37. S. Liu, X. Sun, B. Peng, H. Su, Z. Mei, Y. Huang, J. Deng, C. Su, L. Fang, L. Liu, J. Electroceram. **37**, 137–144 (2016)
38. J. Deng, L. Liu, X. Sun, S. Liu, T. Yan, L. Fang, B. Elouadi, Mater. Res. Bull. **88**, 320–329 (2017)
39. F. Han, S. Ren, J. Deng, T. Yan, X. Ma, B. Peng, L. Liu, J. Mater. Sci.: Mater. Electron. **28**, 17378–17387 (2017)
40. G. Li, Z. Chen, X. Sun, L. Liu, L. Fang, B. Elouadi, Mater. Res. Bull. **65**, 260–265 (2015)
41. X. Sun, J. Deng, S. Liu, T. Yan, B. Peng, W. Jia, Z. Mei, H. Su, L. Fang, L. Liu, Appl. Phys. A **122**, 864 (2016)
42. Y. Huang, L. Liu, D. Shi, S. Wu, S. Zheng, L. Fang, C. Hu, B. Elouadi, Ceram. Int. **39**, 6063–6068 (2013)
43. S. Zheng, D. Shi, L. Liu, G. Li, Q. Wang, L. Fang, B. Elouadi, J. Mater. Sci.: Mater. Electron. **25**, 4058–4065 (2014)
44. L. Sun, R. Zhang, Z. Wang, E. Cao, Y. Zhang, L. Ju, J. Alloys Compd. **663**, 345–350 (2016)
45. L. Singh, U.S. Rai, K.D. Mandal, A.K. Rai, Appl. Phys. A **112**, 891–900 (2013)
46. L. Singh, U.S. Rai, K.D. Mandal, J. Alloys Compd. **555**, 176–183 (2013)
47. J. Jumpatam, A. Mooltang, B. Putasaeng, P. Kidkhunthod, N. Chanlek, P. Thongbai, S. Maensiri, Ceram. Int. **42**, 16287–16295 (2016)
48. J. Deng, X. Sun, S. Liu, L. Liu, T. Yan, L. Fang, B. Elouadi, J. Adv. Dielectr. **06**, 1650009 (2016)
49. F. Han, J. Deng, X. Liu, T. Yan, S. Ren, X. Ma, S. Liu, B. Peng, L. Liu, Ceram. Int. **43**, 5564–5573 (2017)
50. X. liu, L. Liu, F. Han, S. Liu, H. Xiang, L. Fang, J. Mater. Sci.: Mater. Electron. **27**, 12128–12133 (2016)
51. L. Liu, H. Fan, P. Fang, X. Chen, Mater. Res. Bull. **43**, 1800–1807 (2008)
52. L. Liu, H. Fan, X. Chen, P. Fang, J. Alloys Compd. **469**, 529–534 (2009)
53. X. Huang, H. Zhang, M. Wei, Y. Lai, J. Li, J. Alloys Compd. **708**, 1026–1032 (2017)
54. S. Jesurani, S. Kanagesan, M. Hashim, I. Ismail, J. Alloys Compd. **551**, 456–462 (2013)
55. S.-Y. Chung, I.-D. Kim, S.-J.L. Kang, Nat. Mater. **3**, 774–778 (2004)
56. P. Thongbai, J. Boonlakhorn, B. Putasaeng, T. Yamwong, S. Maensiri, J. Am. Ceram. Soc. **96**, 379–381 (2013)
57. Y. Jiancong, L. Yuan-Hua, L. Huafei, C. Bo, N. Ce-Wen, J. Am. Ceram. Soc. **94**, 1966–1969 (2011)
58. L.J. Liu, L. Fang, Y.M. Huang, Y.H. Li, D.P. Shi, S.Y. Zheng, S.S. Wu, C.Z. Hu, J. Appl. Phys. **110**, 6 (2011)
59. L. Liu, Y. Huang, Y. Li, D. Shi, S. Zheng, S. Wu, L. Fang, C. Hu, J. Mater. Sci. **47**, 2294–2299 (2012)
60. W. Somphan, P. Thongbai, T. Yamwong, S. Maensiri, Mater. Res. Bull. **48**, 4087–4092 (2013)
61. D.C. Sinclair, T.B. Adams, F.D. Morrison, A.R. West, Appl. Phys. Lett. **80**, 2153–2155 (2002)
62. Q. Zheng, H. Fan, C. Long, J. Alloys Compd. **511**, 90–94 (2012)
63. J. Boonlakhorn, P. Thongbai, B. Putasaeng, T. Yamwong, S. Maensiri, J. Alloys Compd. **612**, 103–109 (2014)